ELSEVIER

Journal of Molecular Catalysis A: Chemical 172 (2001) 193–206

JOURNAL OF MOLECULAR CATALYSIS A: CHEMICAL

www.elsevier.com/locate/molcata

A molecular mechanism for Fischer–Tropsch catalysis

M.K. Carter*

Carter Technologies, P.O. Box 1852, Los Gatos, CA 95031, USA

Received 10 November 2000; received in revised form 29 January 2001; accepted 29 January 2001

Abstract

The catalysts $Co(HCN)_2$–$Fe(HCN)_2$–$Co(HCN)_2$ and $[Fe(HCN)_2]_3$ were designed, produced and proven for Fischer–Tropsch conversion of synthesis gas to liquid, and waxy aliphatic hydrocarbons, respectively. Hydrocarbons formed upon exposure of the catalysts to synthesis gas at room temperature and above. Hydrogen cyanide, released from the catalysts, was shown by direct MS measurements to be converted initially to nitriles. Thus, hydrogen cyanide became an in situ model compound illuminating a C_1 molecular insertion mechanism. This mechanism accounted for all products. FTIR and GC–MS measurements indicated the type and distribution of liquid hydrocarbons produced. Linear hydrocarbons formed from CO/H_2 while branched hydrocarbons formed from a mixture of acetylene plus CO/H_2 demonstrating the initial C_1 species associated with the catalyst, whether it was CO, HCN or one carbon of acetylene, acted as both tether and terminus in the step-wise chain growth mechanism.

Keywords: Fischer–Tropsch; Linear backbone; Catalysis; Molecular mechanism; Transition metal

1. Introduction

The nature of the molecular mechanism for Fischer–Tropsch (F–T) catalytic conversion of synthesis gas to hydrocarbons has been the subject of investigation for over 70 years [1]. Mechanisms have been proposed assuming multiple sites [2], metal hydrides [3–7], metal alkydes [8], metal clusters [9] and cyclic formyl intermediates [10]. Brady and Pettit [11,12] offered a methylene insertion mechanism based on product distributions which showed striking similarities to products from CH_2N_2/H_2. A fundamental effort, proposed fundamentals of catalysis [13], developed the principles and presented six steps applicable for design of efficient catalysts at the molecular level. The six-step process directs design of the composition and geometry of a catalyst molecule in sufficient detail to afford its production in the laboratory. Such catalysts are believed to be nearly optimal for their specified chemical reactions. The present work is an application of the fundamental development effort and demonstrates catalytic conversion of synthesis gas to liquid aliphatic hydrocarbons using Co–Fe–Co and to wax using Fe–Fe–Fe molecular string type catalysts [13]. A C_1 molecular mechanism is presented for CO insertion at the active catalytic site that accounts for the products. Direct MS measurements and other experimental data are provided in support of the proposed mechanism.

A number of interesting CO bonding investigations have been conducted previously to illuminate the nature of carbon monoxide participation in metal catalyzed F–T hydrogenated carbonylations. One FTIR study proposed the carbonyl band located at $\nu(CO) = 2050\,cm^{-1}$ represented the active mono-carbonyl species on a $Ru–RuO_x/TiO_2$ catalyst in hydrogen [14]. MO calculations for dissociation of CO on the

* Tel.: +1-408-356-6693; fax: +1-408-356-9633.
E-mail address: mkcarter@ix.netcom.com (M.K. Carter).

1381-1169/01/$ – see front matter
PII: S1381-1169(01)00080-2

100 face of Fe_{12} crystals indicated experimentally observed acceleration of CO dissociation on metal catalysts by hydrogen most likely occurred through hydrogen atom attack on the C atom of the absorbed CO molecule [15]. In addition, isotopic evidence of dissociative CO and ^{13}CO adsorption on Rh/zeolite by IR spectroscopy indicated [16] formation of an M–CO bond. Group VIII metals have been shown to be especially active [17,18] for F–T catalysis of CO at temperatures as low as 100°C. There is also evidence of side-on bonding [19,20] between the carbon atom of a carbonyl group and the sterically restricted binuclear manganese complex in $(OC)_2Mn(PH_2PCH_2PPh_2)_2(\mu CO)Mn(CO)_2$. Similar bonding has been reported for a CN analogue having a μ-$CNC_6H_4CH_3$ ligand [21]. These experimental measurements affirm the conditions for which a π-associated CO molecule may form a σ-bond with the catalytic metal site.

Formyl–metal intermediates have been proposed for F–T catalysis. Ru–Co bimetallic clusters on silica have been reported [22] to catalyze CO hydrogenation to C_1–C_5 alcohols. Higher Co/Ru ratios increased activity in reactions for which an IR study showed CO was activated and formyl intermediates were promoted. IR spectra have been reported for adsorbed species on a Rh catalyst using a diffuse reflectance catalytic cell at actual F–T reaction conditions [23]. These authors proposed a formate intermediate in methanation reactions. Mechanistic studies conducted for $CH_3Mn(CO)_5$ and related compounds [24], using a ^{14}CO tracer, have shown the acyl carbonyl to be derived from a coordinated CO such that $CH_3Mn(^{14}CO)_5 + CO \rightarrow CH_3(^{14}CO)Mn(CO)(^{14}CO)_4$ indicating an associated ^{14}CO becomes inserted in the Mn–CH_3 bond. Carbon monoxide insertion has also been studied on a Rh catalyst using IR [25]. In the present work it will be shown that HCN, CO and C_2H_2 follow a C_1 insertion mechanism in F–T catalysis that describes the observed products.

2. Catalyst considerations

F–T catalysts, of the form $Co(HCN)_2$–$Fe(HCN)_2$–$Co(HCN)_2$, have been designed at the molecular level using a six step process based on fundamental considerations developed previously [13]. Those six steps are applied as follows. An acceptable C_1 insertion mechanism was established and the guest reactant molecules, carbon monoxide and hydrogen cyanide, were identified (step 1). Iron (Fe) was selected as the catalytic site (as discussed in the following paragraph) for the Co–Fe–Co backbone or string for which the electronegativity value of Co is slightly greater than that of Fe (step 2) and an $Fe(CO)_4$ bonding energy to associated carbon monoxide reactants of −58 kcal/mol (−243 kJ/mol) was computed (step 3). The first valence state for which the energy values were doubly degenerate was zero (step 4) so that no anions were required (step 5). The rule of 18 was met as neutral iron contributed six 3d-electrons and two 4s-electrons, each of four hydrogen cyanide (or carbon monoxide) associated with the iron atom contributed two 2p-electrons and each cobalt atom may contribute the remaining electrons as 3d-electrons for a total valence set of 18 electrons (step 6). Thus, no additional ligands were required for the catalyst or the precursor. An approximate associated bond energy for the reactant CO associated with the full catalyst was computed by an extended Hueckel method as −14 kcal/mol (−59 kJ/mol). Alternatively, this same process also selected the more common $Fe(HCN)_2$–$Fe(HCN)_2$–$Fe(HCN)_2$ or Fe_3 type catalyst and others as discussed in Section 4.5. The catalyst was made by reducing $Co(CN)_2$–$Fe(CN)_2$–$Co(CN)_2$ in hydrogen rich synthesis gas.

Catalyst, metal string, selection was made based on simple extended Hueckel molecular energy computations referenced to a Hartree–Fock computation for iron tetracarbonyl. Bond energies were computed for strings of first row transition metals associated with carbon monoxide [13]. An 11 atom model consisting of a three-atom string of transition metals associated with four carbon monoxide molecules was considered in which the bond distances of the associated carbon monoxide molecules were optimized for symmetrical bonding to the central metal atom in C_{4v} symmetry. An Fe–Fe bond distance of 2.494 Å was selected while an Fe–C and Fe–O bond distance of 1.95 Å was selected based on averages of X-ray crystallographic measurements [26]. These metal to CO bond distances ranged from an average of 1.87 to an average of 2.24 Å, similar in value to a related computation [27]. A bond distance of 1.30 Å was selected for the C–O bond based on the averages of X-ray crystallographic

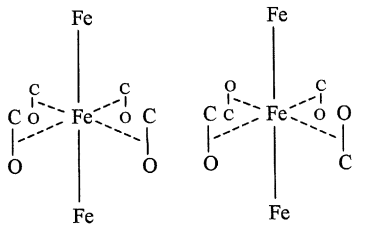

Fig. 1. Representation of Fe–Fe(C–O)$_4$–Fe In C_{4v} symmetry (left) and D_{2d} symmetry (right).

measurements [28,29]. These same bond distances were applied for computation of all first row transition metal atoms. The initial series of computations was conducted for both radial configurations (D_{4h} symmetry group), where the carbons were pointed toward the central iron and, alternatively, the oxygens were pointed toward the central iron. In addition they were conducted for a parallel axis configuration (C_{4v} symmetry group) where all four carbon monoxide molecules were oriented in the same direction with axes parallel to the central metal string axis. The parallel axis configuration was shown to exhibit bonding in the correct range while the radial configurations did not. This is different from the sterically restricted iron pentacarbonyl where iron is bonded to the carbon atoms and the oxygen atoms are extant. Relative zero bond energies were computed for each complex where the carbon monoxide molecules were removed 10 Å from the iron string in their same orientations. In addition, another model was established for carbon monoxide molecules positioned in an alternate anti-parallel orientation [13] (Fig. 1). Again the same set of bond distances was employed. The highest filled levels were within 0.2 eV or 5 kcal/mol of being two-fold degenerate (Table 1). The bonding energy of the Fe–Fe–Fe string complex was improved by −2.34 eV in the alternate anti-parallel configuration, the Cr–Cr–Cr complex was improved by −0.887 eV, the V–V–V was improved by −0.008 eV and the Ni–Ni–Ni complex was improved by −2.856 eV. The bonding energies of the other complexes became weaker ([30]) for other examples of designed symmetric catalysts.

The standard parallel transition metal carbonyl configuration produced five bonding complexes, for which the Mn–Mn–Mn complex displayed the strongest bonding energy. The alternate anti-parallel configuration produced four bonding complexes for which the Fe–Fe–Fe complex displayed the strongest bonding energy. In addition, the standard parallel Co–Fe–Co complex was acceptable for catalyst formation. Energy computations were also conducted for the standard parallel tri-iron string carbonyl configuration as a chloride complex, specifically $Fe_3(CO)_4Cl_8^{4-}$, for which the bonding energy improved by −2.2 eV over the bare eleven element complex. This indicated most of the transition metal string complexes might perform as F–T catalysts. The Co–Fe–Co complex was chosen because it was believed the higher electronegativity of cobalt might increase chain termination rate and produce liquid hydrocarbons as was observed rather than oligomeric waxes.

3. Experimental

Several FT catalysts were prepared for conversion of synthesis gas to hydrocarbons. Catalytic reactions

Table 1
$M_3(CO)_4$ bond energies for first transition metal series elements

Transition metal string	Bond energy (eV) (parallel C–O)	Bond energy (eV) (alternate anti-parallel C–O)
Ti–Ti–Ti	+0.898	+1.105
V–V–V	−0.177	−0.185
Cr–Cr–Cr	+0.292	−0.595
Mn–Mn–Mn	−2.558	+2.812
Fe–Fe–Fe	−0.161	−2.504
Co–Co–Co	−0.141	+2.789
Ni–Ni–Ni	+3.718	+0.862
Cu–Cu–Cu	−0.896	−0.226
Co–Fe–Co	−0.061[a]	+2.674

[a] The Fe–CO bond distance was 1.90 Å.

were conducted at 18–20, 100 and 200°C at gas pressures up to 300 psig. These reactions ran for times of a few hours to more than a week. The data for these catalytic reactions are reported in Section 3.3.

3.1. Catalyst preparation

All steps in the catalyst preparation have been conducted using nitrogen sparging and nitrogen blanketing in sealed plastic containers to minimize air oxidation of the transition metal compounds. A 9.0 g portion of 0.3–0.6 cm silica gel support, previously acid washed to remove trace metals and treated to leave a 3.5% phosphoric acid residue, was transferred into a 1 l vacuum filter flask. A solution of 1.526 gm of $K_4Fe(CN)_6{\cdot}3H_2O$ dissolved in 12 ml of nitrogen purged distilled water was added to and absorbed by the silica gel support. The mixture was dried under vacuum at 35°C for several hours as low valent iron compounds are known to oxidize in air. When dry a second solution containing 1.714 g of $CoCl_2{\cdot}6H_2O$ (or 1.470 g $FeCl_2{\cdot}4H_2O$ to form the Fe_3 type catalyst), dissolved in 12 ml of nitrogen purged DI water, was added. The wet mix was permitted to react with re-dissolved $K_4Fe(CN)_6$ for 5 min as the product precipitated out on the silica support, was drained, washed with two 20 ml portions of nitrogen purged water, drained again and dried as before producing a deep teal blue-green colored solid. The same compound was also prepared without the silica gel support. In addition, a sample of $K_4Fe(CN)_6$ was prepared on silica gel as was a sample of $CoCl_2$. The resultant Co–Fe–Co catalyst was used for all reactions except the waxy solid product, which was formed by the Fe–Fe–Fe catalyst.

3.2. Physical measurements

Three sharp FTIR absorption bands were measured for the catalyst compound with no silica gel support at 2080, 600 and 465 wave numbers indicating ionic bonding of the –CN groups [31,32]. The product, which had been rinsed and dried, was most probably composed of a mixture of insoluble compounds so standard purification procedures were not possible and the original mixture was analyzed as prepared. Elemental analyses of the unsupported compound believed to be $Co_2Fe(CN)_6{\cdot}2H_2O$ was calculated using a model of the most probable mixture (Table 2).

Elemental concentrations indicate production of 66% of the catalyst precursor $Fe(CN)_2$–$[Co(CN)_2]_2{\cdot}2H_2O$. This product was insoluble in hot concentrated hydrochloric and nitric acids, even at elevated pressures and temperatures in a microwave digestion reactor. It was insoluble in hot concentrated sulfuric acid at atmospheric pressure followed by subsequent drop wise additions of 1:1 nitric acid. This is uncharacteristic for mono-metal, transition metal cyanides. It was readily digested in a molten 1:8 mixture of sodium nitrate in sodium hydroxide.

Catalysts were also prepared as described above for use in direct mass spectroscopic measurements except 70–200 micron silica, with surface area of 500 m^2/gram, was substituted for the 0.3–0.6 cm silica gel support. Direct MS measurements were made with this material loaded into 8 in. long by 1/4 in. OD stainless steel tubes. Measurements were conducted using a residual gas analyzer. The MS system was baked under vacuum and a clean background established. One catalyst tube was exposed to 50 psi of unfiltered, premixed 99.998% synthesis gas (33% CO, 67% H_2, <5 ppm O_2 as supplied by a gas vendor) for 30 s at RT. This premixed synthesis gas was used for all reactions. It was cooled to −78°C and all unreacted synthesis gas was removed under a vacuum of 10^{-6} to 10^{-7} Torr. At 45°C mass peaks were detected at 26, 27 Da for HCN.

A second set of MS measurements was conducted for the catalyst exposed to 50 psi synthesis gas for 5 min at RT, cooled to −78°C and all unreacted synthesis gas removed under a vacuum of 10^{-6} to

Table 2
Model of mixed catalyst compounds representing $Fe(CN)_2$–$[Co(CN)_2]_2{\cdot}2H_2O$

	C	N	Co	Fe	H
Experimental weights (anal.)	0.1913	0.2223	0.2188	0.1851	0.0087
Calculated weights for the compounds (calcd.) $0.66[Co(CN)_2]_2$–$Fe(CN)_2{\cdot}2H_2O$ + $0.34[Fe(CN)_2OH]_2$-3KCN	0.1943	0.2266	0.2159	0.1851	0.0089

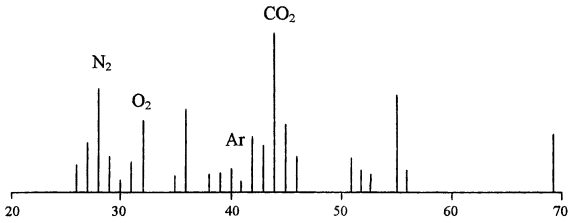

Fig. 2. MS spectrum of catalyzed synthesis gas at 45°C (50 psi for 5 min).

10^{-7} Torr. At 45°C mass peaks were detected at 26, 27 Da (HCN), 29, 30 Da (C_2H_6), 42, 43, 44 Da (C_3H_8), and 51, 52, 53 Da (CH_2=CHCN) (Fig. 2) for a reconstruction of the MS. Atmospheric gases and hydrocarbon fragments were indicated at low levels and there appeared to be several contributions to mass 44. Methane was not detectable at a concentration greater than the combined contributions from other ions. At 60°C additional mass peaks were detected at 69, 68 Da (C_3H_7CN), 83, 82, 81 Da (C_4H_9CN), 58, 57, 56 Da (C_4H_{10}), 60, 59, 58 Da (C_3H_7OH), 72, 71, 70 Da (C_5H_{12}), 74, 73, 72 Da (C_4H_9OH), 86, 85, 84 Da (C_6H_{14}), plus indications of methylacetamide and a cycloalkene alcohol. These assignments were based on the measured mass values where only the elements C, H, N and O were present. Finally, another catalyst tube was exposed to pure hydrogen gas using the same set of conditions as before. Upon warming to between 25 and 60°C none of the previously reported products were detected indicating that cyanide remained associated with the catalyst.

3.3. Reaction results

Five different catalytic conversions of synthesis gas to products using the $Fe(CN)_2$–$[Co(CN)_2]_2$ catalyst are reported. One of these reactions employed both acetylene and synthesis gas as reactants. In addition, synthesis gas conversions were attempted using $K_4Fe(CN)_6$ and $CoCl_2$ separately absorbed onto silica gel, prepared as before and run at 18–20°C up 300 psig but no measurable synthesis gas was absorbed and no products were recovered demonstrating neither mono-metal reactant was catalytic for F–T conversions.

Catalytic reactions were conducted in a static mode using a 30 cm long by 1.2 cm diameter vertical, heated, 304 stainless steel (ss) reactor. The reactor was pressure tested to assure it to be leak free. The reactor was loaded with 1 mmol of catalyst supported on 2.0–2.5 g of silica gel under a nitrogen blanket for each reaction. This catalyst loading procedure may have exposed some of the catalysts to air resulting in possible variations in reaction rates. The catalyst was flushed three times with 50 psi synthesis gas and pressurized to 0.69–2.07 MP (100–300 psig). Gas consumption, which began upon vessel closure, was monitored by recorded decreases in pressure as a function of time. The reaction represented by data in Table 3 was run at 18°C with a 125 ml reactor volume. After just over 25 h 1.1 g of a liquid hydrocarbon sample was isolated. The reaction of data in Table 4 was run at 20°C with a 65 ml reactor volume. After just over 2 h approximately 0.4 g of a liquid hydrocarbon sample was isolated. The reaction of data in Table 5 was run at 100°C with a 65 ml reactor volume. After more than three quarters of an hour approximately 0.1 g of a liquid hydrocarbon sample was isolated. The reaction of data in Table 6 was run at 200°C with a 65 ml reactor volume. After more than three quarters of an hour approximately 0.07 g of a liquid hydrocarbon sample was isolated. Synthesis gas additions were made following pressure drops of approximately 100 psig. The reaction of data in Table 7 was run at 18°C with a 125 ml reactor volume. This reaction was conducted by pressurizing the reactor with 22 psig acetylene followed by filling to 150 psig with synthesis gas. After just over 7 days 2.4 g of a liquid hydrocarbon sample was isolated.

The indicated reaction rate for data of Table 3 run at 18°C was approximately 44 g product per mole of catalyst per hour. Upon warming the catalyst exposed

Table 3
FT catalytic formation of liquid hydrocarbons at 18°C: added approximately 1 mmole catalyst on 2.1 g of silica support (reactor volume = 125 ml)[a]

Time (min)	Pressure (psi)	CO consumed (mmol)
0	245	–
6	205–252	5
14	175–300	14
44	155–300	31
702	19–305	64
1502	24	97

[a] The 0.097 mole of CO produced 1.11 g of liquid hydrocarbon.

Table 4
FT catalytic formation of liquid hydrocarbons at 20°C: added catalyst on 2.4 g of silica support (reactor volume = 65 ml)[a]

Time (min)	Pressure (psi)	CO consumed (mmol)
0	250	–
7	198	3
11	177	4
12	173	4
16	140	7
20	108–250	9
26	212	11
36	170	14
41	139	15
46	101–250	18
50	228	19
56	199	21
69	158	23
75	144	24
83	99–250	27
92	215	29
103	184	31
131	131	34

[a] The 0.034 mole of CO produce approximately 0.4 g of liquid hydrocarbon.

to 300 psig synthesis gas the apparent reaction rate decreased indicating loss of activity (possibly due to the presence of the byproduct water). The indicated reaction rate at 18°C for 85% synthesis gas and 15% acetylene was approximately 13 g product per mole of catalyst per hour (see data in Table 7).

Brief exposure to ambient air occurred during catalyst transfers to the reactor that caused variability in measured catalyst activity.

In a separate experiment the catalyst was exposed to synthesis gas at 50 psig for 15 s at 18°C followed by an immediate addition of a measured volume of distilled water. The cyanide concentration of the recovered water, as measured by IC, accounted for 112% of the cyanide anticipated from $Fe(HCN)_2$–$[Co(HCN)_2]_2$.

Table 5
FT catalytic formation of liquid hydrocarbons at 100°C: added catalyst on 2.4 g of silica support (reactor volume = 65 ml)[a]

Time (min)	Pressure (psi)	CO consumed (mmol)
0	250	–
2	243	0.3
4	233	0.8
6	224	1.3
8	217	1.6
13	199	2.5
16	189	2.9
19	180	3.4
21	174	3.7
24	167	4.2
27	149–250	4.9
30	239	5.4
33	230	5.8
36	219	6.4
40	205	7.0
45	192	7.7
49	182	8.1

[a] The 0.0081 mole of CO produce approximately 0.1 g of liquid hydrocarbon.

Table 6
FT catalytic formation of liquid hydrocarbons at 200°C: added approximately 1 mmole catalyst on 2.0 g of silica support (reactor volume = 65 ml)[a]

Time (min)	Pressure (psi)	CO consumed (mmol)	Pressure (psi)
0	250	–	0
11	211	1.5	39
21	181	2.6	69
35	150–250	3.8	100
46	220	4.9	130
54	201	5.7	149

[a] The 0.0057 mole of CO produce approximately 0.07 g of liquid hydrocarbon.

Table 7
FT catalytic formation of liquid hydrocarbons at 18°C: added approximately 1 mmole catalyst on 2.5 g of silica support (reactor volume = 125 ml); charged reactor with 22 psi acetylene then to 150 psi synthesis gas[a]

Time (h)	Pressure (psi)	CO consumed (mmol)
0	150	–
0.3	18–150	15
3	65	26
22	<5–150	33
48	23–150	48
59	29–150	63
72	27–150	77
83	29–150	92
97	26–150	107
105	36–150	120
119	26–150	135
131	30–150	149
144	29–150	163
155	32–150	180
168	29–150	194
172	<10	211

[a] The 0.21 mole of CO produced 2.4 g of liquid hydrocarbon.

Prepared catalysts were immediately active, requiring no pretreatment or activation conditions, indicating the compound that formed in hydrogen rich synthesis gas was the active species. Catalyzed reaction data (Table 7), run for more than a day without addition of synthesis gas, indicated the pressure decreased to less than 0.034 MP (<5 psig). This implied little or no gaseous hydrocarbon products were formed. Condensed hydrocarbon products were isolated by opening the reactor to air, removing the catalyst with products to a glass beaker and thoroughly extracting the silica gel catalyst support by vigorously boiling reagent grade dichloromethane solvent. The resultant solution was transferred to a glass vial and the solvent was evaporated leaving the oily liquid products. Isolated hydrocarbon products consisted of oily liquids containing some waxy solids. Gaseous products, if formed, were not isolated. One reaction, run using an Fe_3 type catalyst at 20°C and 100–300 psig gas, produced approximately 0.1 g of a waxy semisolid similar to products reported for microcrystalline iron catalysts [33]. No further measurements were conducted for the waxy semisolid.

3.4. FTIR and GC–MS measurements

FTIR and GC–MS analyses of the isolated hydrocarbon products provided structural information. An FTIR spectrum was run (Fig. 3) for the sample reported in Table 3 showed the products to be aliphatic hydrocarbons with absorption bands located at 2920 ($–CH_3$ stretch), 2850 ($–CH_2–$ stretch), 1470 ($–CH_2–$ deformation), 1385 ($–CH_3$ deformation) and 725 ($–(CH_2)_4–$ crankshaft rotation) wave numbers [31,32]. Presence of the 725 wave number band and the essential absence of side chain methyl branching bands indicated the hydrocarbons contained at least C_4 linear sections with no indications of branching. There were also weak absorption bands at 1725 wave numbers indicating a carbonyl group and an –OH stretch at 1085 wave numbers in agreement with the direct MS observation.

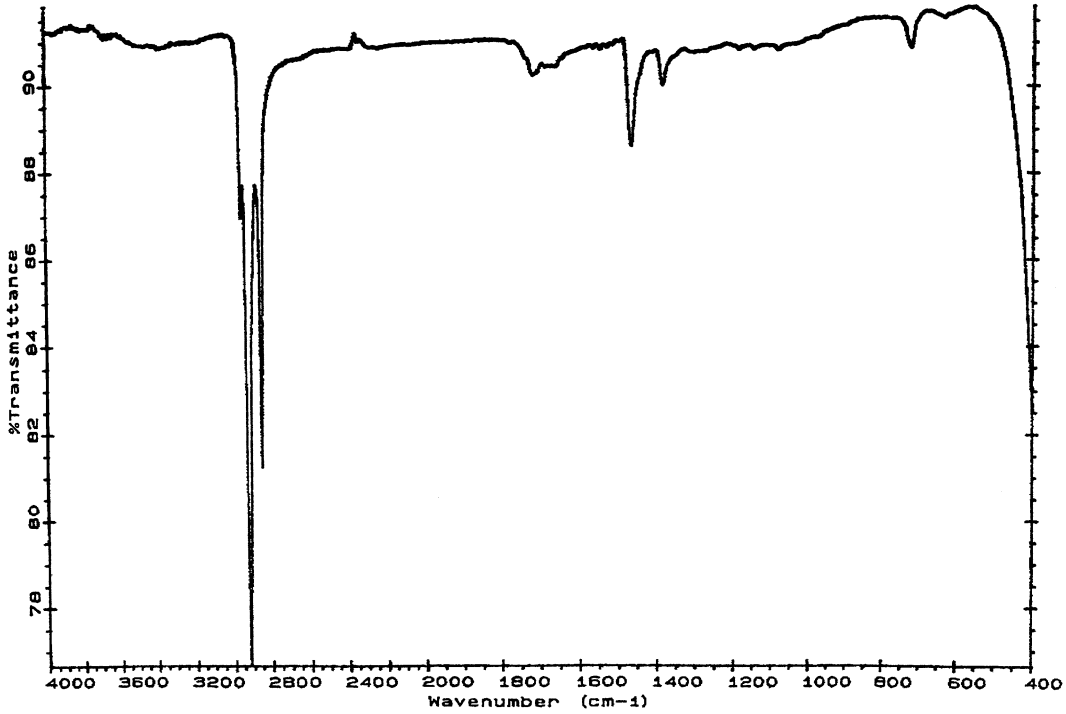

Fig. 3. An FTIR spectrum of linear hydrocarbon liquids formed by FT catalysis.

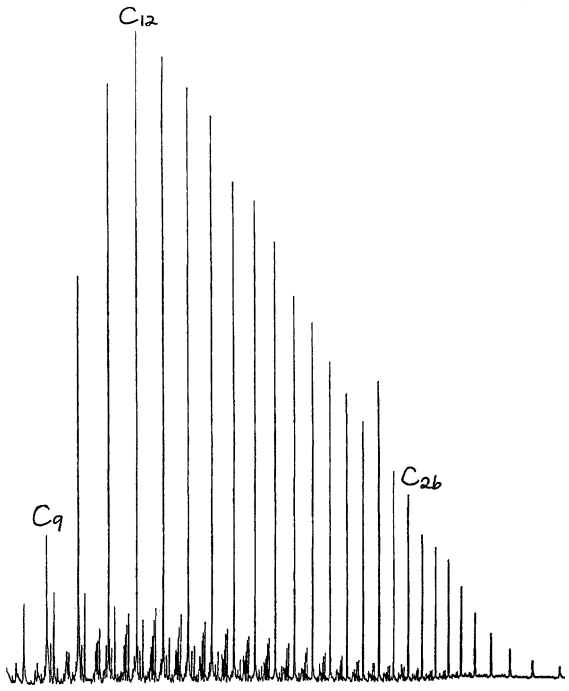

Fig. 4. A GC–MS chromatogram of hydrocarbon liquids formed by FT catalysis.

A GC–MS elution chromatogram (Fig. 4) of the condensed hydrocarbon products reported in Table 3 showed significant aliphatic hydrocarbon peaks at regular C_1 intervals beginning with C_8, exhibiting a maximum at C_{12} and decreasing in intensity to C_{35}. Mass spectroscopic analysis identified the major peaks as the linear aliphatic hydrocarbons octane (C_8), nonane (C_9), decane (C_{10}), endecane (C_{11}), dodecane (C_{12}), eicosane (C_{20}), etc. This product distribution has a maximum in the liquid range as compared to the solid products produced from the extensive work of Kuo [33], and many others, using microcrystalline iron catalysts. Minor peaks, which were positioned between the hydrocarbon peaks, accounted for approximately 8% of the 1.1 g of products produced from 1 mmol of catalyst. These compounds were identified by mass spectroscopy as nitrogen and oxygen substituted hydrocarbons as α-nitriles (category 1), amides (category 2), alcohols and ketones (category 3), and unsaturated cyclic compounds (category 4). Some of the lower molecular weight compounds identified in category (1) were acetonitrile, propionitrile and butyronitrile. In category (2) *N*-methyl formamide and *N*,*N*-dimethyl formamide were found. In category (3) hexanones and a heptanol were observed and in category (4) cyclohexenols and cyclohexenones were detected in agreement with the direct MS data.

The conversion run using a mixture of 85% synthesis gas and 15% acetylene also produced liquid hydrocarbons (Table 7). An FTIR spectrum (Fig. 5) of the resulting liquid showed the products to contain branched aliphatic hydrocarbons with absorption bands located at 2960 ($-CH_3$ stretch), 2925 and 2850 ($-CH_2-$ stretch), 1462 ($-CH_2-$ deformation), 1380 ($C-CH_3$ deformation), 1260 ($RC-(CH_3)_3$), 1190 ($C-(CH_3)_{2,3}$), 1175 and 1150 ($C-(CH_3)_2$), 805 ($CH-(CH_3)_2$, and 720 $-(CH_2)_4-$ wave numbers. In addition, a substituted ketone carbonyl stretch absorption band was observed at 1765 wave numbers, cyclohexane skeletal mode bands were observed at 1025, 978 and 875 wave numbers [34], an aliphatic amide band was observed near 1650 wave numbers (–NH deformation), nitrile and cyanide bands were detected at 2240, 2065 and 2020 wave numbers, and possible alcohol bands were detected at 1095 and 1070 wave numbers. The bands located at 1260, 1190, 1175, 1150 and 805 wave numbers all represent branched methyl group motions. This molecular bonding configuration was substantially different from the linear hydrocarbons formed without use of acetylene.

A GC–MS elution chromatogram (Fig. 6) of hydrocarbon products presented in Table 7 showed significant peaks at regular C_1 intervals beginning with C_9, exhibiting a maximum in the liquid range at C_{16}, rapidly decreasing in intensity to C_{25} and terminating at C_{36} which when analyzed showed the presence of both linear, and branched aliphatic hydrocarbons. Minor peaks, which were positioned between the hydrocarbon peaks, accounted for approximately 3.5% of the 2.4 g of products produced from 1 mmol of catalyst. Both GC–MS spectral analyses (samples of Tables 3 and 7) account for approximately 0.08 g of non-hydrocarbon products formed indicating the same fixed amount of cyanide from the 1 mmol of catalyst. These compounds were identified by mass spectroscopy as nitrogen and oxygen substituted hydrocarbons as before. Since the relative concentration of the minor nitrogen containing compounds decreased significantly with increasing product mass (compare Fig. 6 to Fig. 4), this indicated they were

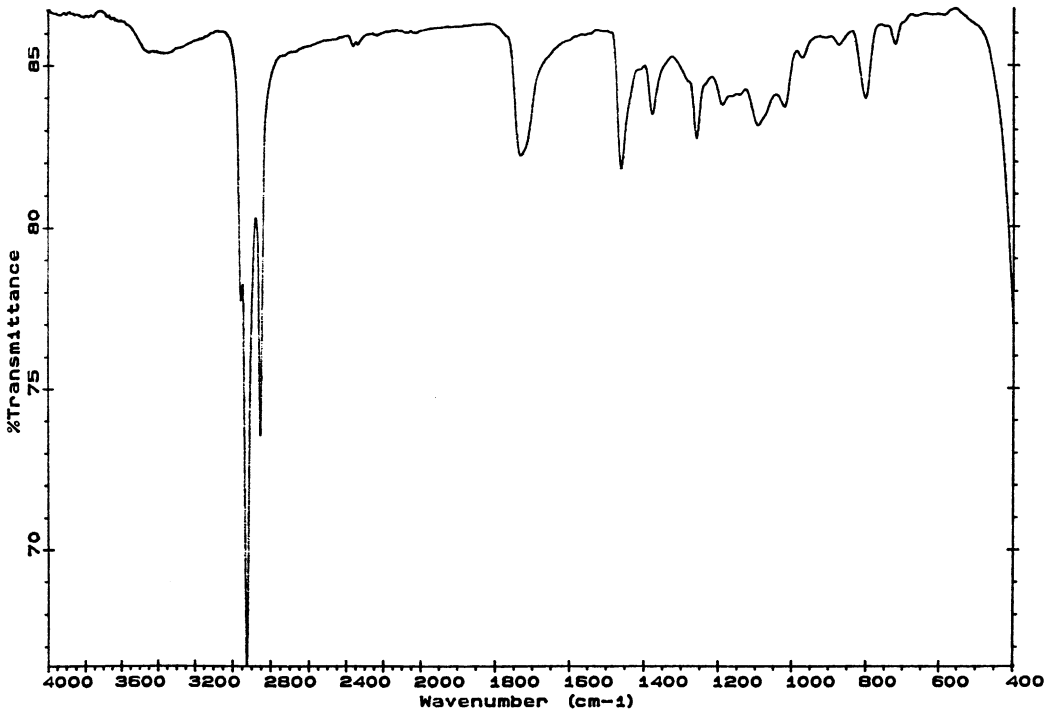

Fig. 5. An FTIR spectrum of branched hydrocarbon liquids formed by FT catalysis of a mixture of synthesis gas and acetylene.

most likely formed by consuming the HCN from the catalyst.

4. Discussion

Fischer–Tropsch catalytic conversion of synthesis gas to hydrocarbons may be represented by the equation

$$(2n+1)H_2 + nCO \overset{\text{catalyst}}{\rightarrow} C_nH_{2n+2} + nH_2O$$

The equation indicates that hydrocarbon products are formed from synthesis gas reactants but it does not provide any mechanistic direction. A significant body of chemical engineering literature exists describing the effects of changing conditions of the reactor, catalyst, process and the balance of CO/H_2 ratio [33]. Optimal sets of process reaction conditions are well established for the crystalline iron catalyst. What has not been established previously is a detailed molecular mechanism of F–T catalysis. Brady and Pettit [11,12], and others [8,10] have presented arguments for hydrocarbon formation by a proposed methylene group insertion mechanism but direct chemical evidence for such an insertion has been illusive. Furthermore, there does not appear to be any rational energy benefit or energy lowering for insertion of a methylene group into an existing saturated hydrocarbon chain. Thus, an alternative mechanism was sought.

4.1. Catalyst formation chemistry

The catalyst of interest is indicated to be formed according to the chemical reaction equation

$$K_4Fe(CN)_6 + 2CoCl_2 \rightarrow$$
$$Co(CN)_2\text{–}Fe(CN)_2\text{–}Co(CN)_2 + 4KCl$$

Exposure to reducing synthesis gas produced hydrocarbons, nitriles and formamides demonstrating cyanide, the only available source of nitrogen present, had been incorporated into the catalytic reaction sequence. Direct MS experiments of products formed

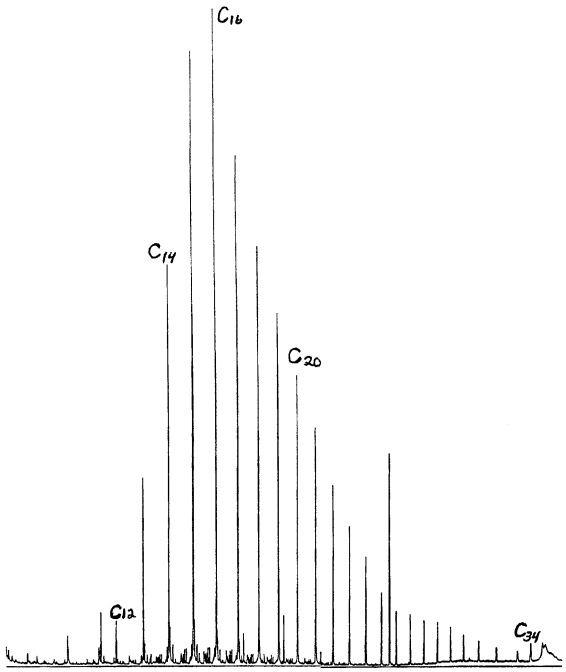

Fig. 6. A GC–MS chromatogram of hydrocarbon liquids formed by FT catalysis of a mixture of synthesis gas and acetylene.

resulting from exposure of the catalyst to 50 psig synthesis gas for 30 s proved HCN was released from the catalyst. This was confirmed by measurement of the expected concentration of HCN upon exposure of catalyst to synthesis gas in the 1.2 cm diameter vertical tube reactor followed by addition of DI water. Formation of HCN is anticipated to occur by reduction of $M(II)(CN)_2$ species to $M(0)(HCN)_2$ as

$$Co(CN)_2\text{–}Fe(CN)_2\text{–}Co(CN)_2 + 3H_2 \xrightarrow{H^+} Co(HCN)_2\text{–}Fe(HCN)_2\text{–}Co(HCN)_2$$

The CO present in synthesis gas is believed to displace HCN as indicated:

$$Co(HCN)_2\text{–}Fe(HCN)_2\text{–}Co(HCN)_2 + 6CO \rightarrow Co(CO)_2\text{–}Fe(CO)_2\text{–}Co(CO)_2 + 6HCN$$

Mass spectral measurements proved the catalyst was active for formation of hydrocarbon products upon exposure to 50 psi synthesis gas at room temperature for 5 min. Furthermore, some of the products formed contained bonded nitrogen that could only have originated from the cyanide ligands. Since the catalyst was washed several times with DI water to remove soluble cyanide compounds then formation of nitriles and formamides indicated cyanide ligands took an active role in product formation. Initial release of hydrogen cyanide upon exposure of the catalyst to synthesis gas, was fortunate in that CO displacement of HCN provided some most interesting evidence relating to the molecular catalytic mechanism. Not only did carbon monoxide react to form hydrocarbons but cyanide must also have been involved in the initial steps of the reaction. Hydrogen cyanide proved to be an in situ model reactant illuminating some of the detailed chemical reaction steps. The cyanide ligands were probably among the first reactants present. Thus, both CO and –CN were incorporated into hydrocarbon products indicating a C_1 molecular mechanism was fundamental to the reaction process.

4.2. Fischer–Tropsch catalysis

A molecular mechanism should describe all main features of a chemical transformation, just as all bands of a molecular spectrum are expected to describe the same subject molecular structure. Should the molecular reaction mechanism have involved free radical reactions it would have caused chain branching at random positions in product molecules [35], whereas appearance of the IR absorption band located at 725 wave numbers indicated the catalyst directed formation of primarily linear aliphatic hydrocarbons as commonly observed in F–T conversions. A near absence of branched methyl skeletal bands supported this conclusion. Therefore, a free radical mechanism was not anticipated. The hydrocarbon product distributions presented in Figs. 4 and 6, do not follow the simple Anderson–Schulz–Flory model. Instead a more complex model, such as the Flory–Schulz or most probable distribution for weight-fraction of product has more degrees of freedom and thus has the capacity to fit or predict the data. However, this model does not necessarily account for the way the products are formed from the string catalysts used in this work.

Much of the previous work [3–5,8–12,36] that focused on elucidating the molecular mechanism of F–T conversions on heterogeneous catalysts proposed

initial formation of methyne and methylene groups. In contrast, previous experimental measurements based upon homogeneous model compounds supported catalytic formation of hydrocarbons from association of a carbon monoxide molecule with an active site [14,16] followed by production of a formyl intermediate [19,20]. Production of formyl intermediates relies on hydrogen reacting with absorbed CO to form a methylene group [15,22] bonded to the catalytic site. Adsorption of a subsequent carbon monoxide molecule has been reported to insert into the established, metal carbon bond [24]. These transition metal compounds, whether found in heterogeneous or homogeneous reactions, would be expected to follow the same consistent bonding model, although product distributions may differ.

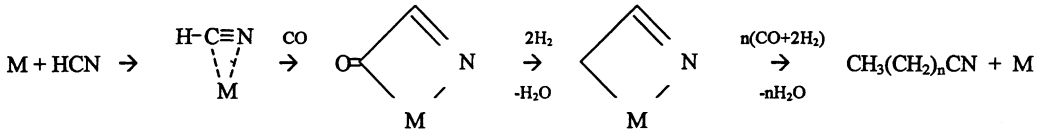

4.3. Bonding evidence

FTIR and elemental analysis data support formation of a $Co_2Fe(CN)_6$ catalyst precursor. Its exposure to synthesis gas for 15 s reduced the compound so hydrogen cyanide was formed according to the reaction given on a previous page. In addition, this was undoubtedly accompanied by reduction of Co and Fe to zero valent species, like the microcrystalline iron catalysts. Exposure to hydrogen gas in the absence of carbon monoxide did not release HCN implying the presence of CO was necessary to coordinate with the transition metals in displacing HCN. Mechanistic studies [24] using a ^{14}CO tracer have shown the acyl carbonyl to be derived from a coordinated CO inserted in the metal alkyl bond. IR studies have also indicated CO insertion for a transition metal catalyst [25]. Direct MS measurements of the saturated hydrocarbons C_2H_6, C_3H_8, C_4H_{10}, C_5H_{12}, and C_6H_{14} formed from synthesis gas using the $Fe(HCN)_2$–$[Co(HCN)_2]_2$ catalyst indicated it is reasonable to expect hydrocarbon formation to follow the same insertion mechanism.

Direct MS measurements showed acrylonitrile, propionitrile, butyronitrile and pentylnitrile were formed. In addition, GC–MS measurements showed formation of alkyl nitriles to be most probably alpha nitriles. This data indicated that HCN was bound to the active transition metal site when CO insertion occurred, generating terminal nitrile products from synthesis gas and residual HCN. Both CO and –CN have 2sp-bond orbitals that became directly involved in a C_1 catalytic mechanism as demonstrated by the following proposed mechanistic reaction sequence.

Nitrile formation, category 1, implies a molecular mechanism based on CO insertion as shown:

Thus, production of nitriles may be accomplished using synthesis gas with addition of HCN. Direct MS measurements also indicated early formation of methylacetamide. Should carbon monoxide have entered the reaction at the M–N bond rather than at the M–C bond then amides, category 2, would be produced as indicated in direct MS measurements. Direct MS measurements also detected the presence of propanol and butanol. These category 3 products can be explained using the same insertion model, as described for category 1, replacing the nitrogen atom by oxygen from CO where the oxygen atom becomes part of the organic products instead of being released as Fe–O at reductive termination. It becomes apparent that propagation requires a repeating sequence of CO insertion followed by H_2 reduction. Should H_2 reduction be followed by another H_2 instead of CO insertion then chain termination would result in formation of a saturated hydrocarbon. Should H_2 reduction be followed by H_2O produced in a prior reaction step then a less favored chain termination mechanism may result in formation of an aliphatic alcohol.

4.4. A C_1 molecular mechanism

Formation of oligomeric aliphatic hydrocarbons from CO/H_2 is expected to follow the same C_1 insertion mechanism MS measurements indicated for HCN as shown in the following reaction sequence.

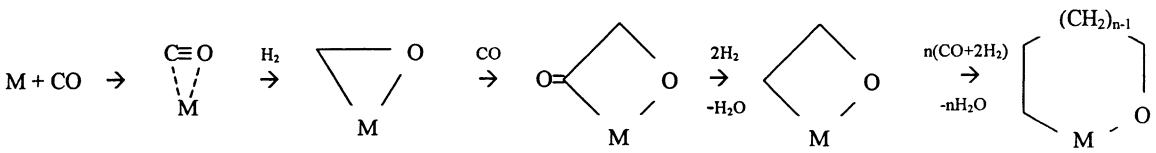

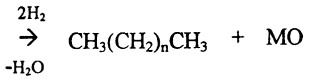

Direct MS measurements showed formation of ethane, propane, butane, pentane and hexane. A low concentration of methane could also have been produced but the other organic compounds masked its identification. Formation of an oxygenated product indicates the growing hydrocarbon may sometimes become terminated without loss of the pendant oxygen atom. Rather, the oxygen atom may be retained forming an alcohol as shown by the direct MS results. At higher reaction temperatures alcohols dehydrate to form alkenes, which are often observed in F–T products resulting from microcrystalline iron catalysts. Formation of a cyclohexenol, category 4, as indicated by MS measurements, implies chain termination can sometimes occur by means of cyclization through condensation.

The C_1 chemical reaction mechanism presented above shows production of linear aliphatic hydrocarbons rather than branched products. This is confirmed in FTIR evidence as a 725 wave number absorption band for un-branched hydrocarbon groups and essential absence of the usual branched methyl bands. Linear hydrocarbons account for more than 90% of the products, but a small amount of branched hydrocarbon (∼5% contribution) was detected. Since the catalytic mechanism does not readily account for their formation it seems possible a few branched hydrocarbons might form during the reduction of an inserted carbonyl group. Should a second carbon monoxide molecule become bonded to a partially reduced carbonyl carbon in place of a second hydrogen atom a methyl branch would be expected to form. Statistical considerations indicate such bonding might occur once per 16 methylene groups formed (∼6% contribution).

The catalyst precursor was converted to the catalyst by carbon monoxide in hydrogen. A near lying or degenerate electronic state favoring sigma-bonds can contribute to the electronic pi-bonding state to provide the first step of the catalytic mechanism, a shift in the pi-bonded ligand to a sigma-bonded –CO– [13]. Once formed, a sigma-bonded –CO– may be readily reduced in hydrogen to form an $–OCH_2–$ or formyl group. Insertion of both carbon monoxide and hydrogen cyanide indicate a C_1 catalytic mechanism to be active. Since –C≡O and –C≡N groups became inserted into growing molecular chains possibly –C≡C– groups could also be inserted as one carbon of acetylene may be considered to be an sp-carbon reactant. Addition of acetylene demonstrated the insertion did indeed occur so that branched chains were produced. Not only did this prove that –C≡C– could be inserted into growing hydrocarbon chains but it also demonstrated a mechanism of C_1 insertion rather than a C_2 insertion to be active. Product formation chemistry for inclusion of acetylene is proposed to follow a quite similar C_1 insertion mechanism, namely

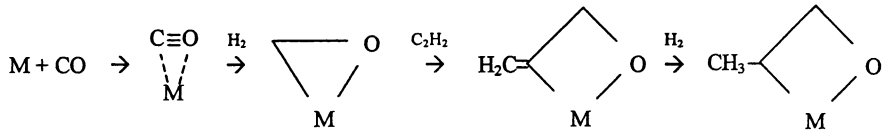

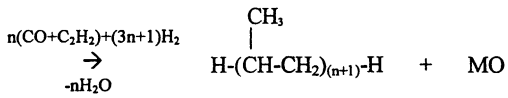

Incorporation of a propyne or other alkyne reactants might be anticipated to produce longer side chain branches than acetylene plus carbon monoxide. Introduction of alkynes and related sp-carbon compounds can afford design of the number and type of branching locations in a growing hydrocarbon. This chemistry offers an opportunity to control the degree of branching and, thus, the product distribution. Elemental C^{13} has been reported to form methane on active F–T catalysts [17,18]. This may also be a result of a C_1 absorption step. Hydrogen cyanide and hydrogen have been reported [36] to produce a minority of gaseous alkanes and alkenes with a majority of nitrogen at 300°C over a microcrystalline iron catalyst. Since HCN can decompose to cyanogen and other products including H_2, N_2 and C at elevated temperatures, it is likely that the majority products may be attributable to this reaction path. Hydrogen cyanide may also form products according to the nitrile formation mechanism proposed for category 1, where alkenes (and alkanes in subsequent hydrogenation) and nitrogen are the anticipated products for this reaction path.

Consideration was given to the possibility that the $FeCo_2$ type catalyst might be present as a transition metal hydride even though carbon monoxide insertion into metal hydride bonds is not well known [24]. Since such hydrides are not normally stable in the presence of water, and since the F–T catalytic reaction produces one water molecule with each methylene group formed it is not probable that such hydrides are present.

Formation of F–T hydrocarbons, as demonstrated by Brady and Pettit [11,12] using diazomethane, may also be explained based upon the proposed C_1 insertion mechanism. This would presume association of the first diazomethane to the active site followed by insertion of subsequent molecules. Since reduction of the nitrogen to amines (or other nitrogen compounds) on Fe could require extreme hydrogen pressure, the by-products are anticipated to be nitrogen gas.

4.5. Alternative catalyst considerations

Liquid aliphatic hydrocarbons are the major products from the F–T catalytic conversion using the $FeCo_2$ type catalyst while waxy solids are produced by Fe_3 type catalyst. Other linear three element type catalyst backbones or strings, including Fe–Mn–Fe, Co–Mn–Co, Ni–Mn–Ni, Ni–Fe–Ni, Co–Fe–Ni, Fe–Mn–Co and others bonded in linear 4p configurations [13] which conform to the electronic requirements are anticipated to produce different product distributions. Polycentered metal carbonyl clusters have been shown to affect F–T catalytic hydrogenation of carbon monoxide in formation of C_3–C_{30} alkanes [9]; good F–T activity has been reported for the Zr–Co–Ni–Cu alloy [37] and other metal clusters such as linear crystalline surfaces or other geometric configurations as found in Mn–Co alloy [38,39], and microcrystalline iron [2,33,40] while monomeric metals were reportedly inactive [41–43].

5. Conclusions

The $FeCo_2(CN)_6$ F–T type catalyst produced liquid aliphatic hydrocarbons in addition to α-nitriles, alcohols and other minor products. Formation of these in situ model compounds has been described as a step-wise C_1 catalytic molecular insertion mechanism wherein carbon monoxide becomes associated with and bonded to the active site. Direct MS measurements indicated the initial C_1 associated with the catalyst, whether it was carbon monoxide, hydrogen cyanide, or one carbon of acetylene, acted as both the tether and terminus in the step-wise chain growth mechanism. This required the initial sp-hybrid bond be transformed to a sp^3-hybrid in the presence of hydrogen. Succeeding additions of the reactant were indicated to occur by an insertion mechanism, at the established metal–carbon bond, with loss of water through hydrogenation. The proposed C_1 catalytic insertion mechanism explained formation of hydrocarbons, alcohols, nitriles, formamides and substituted cyclic alkenes. It is suggested that catalytic polymerization of diazomethane in hydrogen reported by Brady and Pettit [11,12] might also be explained by this mechanism.

More work is needed to determine the optimal conditions and limits of the F–T reaction for direct formation of liquid aliphatic hydrocarbons. F–T single process step catalytic conversion of coal gases to liquid hydrocarbons is inherently less expensive than a two step process. Many new catalysts are yet to be tested while questions regarding limits of the reaction mechanisms, impurity influences on stability and activity of the catalysts also need to be addressed. It is hoped that this work will encourage more investigative

activity toward understanding the molecular electronic mechanism of catalysis in general, as well as motivating a more detailed investigation of the F–T mechanism specifically.

Acknowledgements

The timely assistance of Dr. Ripudaman Malhotra of SRI, International with direct MS measurements was appreciated.

References

[1] F. Fischer, H. Tropsch, Brennstoff Chem. 4 (1923) 276.
[2] M.E. Dry, Ind. Eng. Chem., Product Res. Dev. 15 (4) (1976) 282–286.
[3] R.S. Armstrong, T. Bell, A.F. Masters, M.A. Williams, A.L. Chaffee, Polyhedron 9 (23) (1990) 282–286.
[4] J.W. Rathke, H.M. Feder, J. Am. Chem. Soc. 100 (1978) 623.
[5] M.E. Dry, Catalysis — Science and Technology (Chap. 4), J.R. Anderson, M. Boudart (Ed.), Springer, New York, NY, 1980.
[6] M.E. Dry, Catal. Today 6 (3) (1990) 623.
[7] J.J. Boor, Polym. Sci., Part D 2 (1967) 115.
[8] P.M. Maitlis, H.C. Long, R. Quyoum, M.L. Turner, Z.-Q. Wang, Chem. Commun. 1–8 (1996).
[9] Masters and Van Doorn UK Patent Application No. 40322-75 (1975).
[10] H. Pichler, H. Schultz, Chem. Ing. Tech. 12 (1970) 1160–1174.
[11] R.C. Brady III., R.J. Pettit, Am. Chem. Soc. 102 (1980) 6181–6182.
[12] R.C. Brady III., R.J. Pettit, Am. Chem. Soc. 103 (1981) 1289–1291.
[13] M.K. Carter, Proposed fundamentals of catalysis, submitted for publication.
[14] N.M. Gupta, V.S. Kamble, R.M. Iyer, K.R. Thampi, M. Gratzel, J. Catal. 137 (2) (1992) 473–486.
[15] G. Blyholder, M. Lawless, Langmuir 7 (1) (1991) 140–141.
[16] P. Gelin, J.-F. Dutel, Y.J. Ben Taarit, Chem. Soc., Chem. Commun. 24 (1990) 1746–1747.
[17] D.J. Dwyer, G.A. Somorjai, J. Catal. 52 (2) (1978) 291–301.
[18] P. Biloen, J.N. Helle, W.M.H. Sachtler, J. Catal. 58 (1) (1979) 95–107.
[19] R. Colton, C.J. Commons, Aust. J. Chem. 28 (1975) 1673–1680.
[20] C.J. Commons, B.F. Hoskins, Aust. J. Chem. 28 (1975) 1663–1672.
[21] L.S. Benner, M.M. Olmstead, A.L. Balch, J. Organomet. Chem. 159 (1978) 289.
[22] A. Fukuoka, F. Xiao, M. Ichikawa, D.F. Shriver, W. Henderson, Shokubai 32 (6) (1990) 68–71; CA 114–64725v.
[23] J.J. Benitez, R. Alvero, I. Carrizosa, J.A. Odriozola, Catal. Today 9 (1/2) (1991) 53–60.
[24] F.A. Cotton, G. Wilkinson, Advanced Inorganic Chemistry, Wiley, New York, 1980, pp. 1250–1251.
[25] G. Srinivas, S.S.C. Chuang, J. Phys. Chem. 98 (11) (1994) 3024–3031.
[26] C.H. Wei, L.F. Dahl, J. Am. Chem. Soc. 91 (1969) 1351.
[27] W.J. Hehre, L. Radom, P.v.R. Schleyer, J.A. Pople, Ab Initio Molecular Orbital Theory, Wiley, New York, 1986, p. 219.
[28] F.A. Cotton, J.M. Troup, J. Am. Chem. Soc. 96 (1974) 3438–3443.
[29] J.I. Ball, C.H. Morgan, Acta Cryst. 23 (1967) 239–244.
[30] M.K. Carter, Catalytic, ambient temperature air oxidation of hydrocarbons, submitted for publication.
[31] L.J. Bellamy, The Infrared Spectra of Complex Molecules, Chapman and Hall, New York, 1975, pp. 27–29.
[32] R.C. Weast, CRC Handbook of Chemistry and Physics, 65th Edition, CRC Press, Boca Raton, FL, 1985, Sect. F, p. 202.
[33] J.C.W. Kuo, Slurry Fischer–Tropsch/mobil two stage process of converting syngas to high octane gasoline, A DOE Contract Report Number DOE/PC/30022-10 (DE84004411), 1983.
[34] J. Sheppard, Inst. Pet. 37 (1951) 95.
[35] S.W. Benson, The Foundations of Chemical Kinetics, McGraw-Hill, New York, 1960, p. 610.
[36] H.W. Buschmann, M. Ritschel, W. Vielstich, J. Catal. 106 (1987) 337–341.
[37] I.R. Harris, I.T. Caga, A.Y. Tata, J.M. Winterbottom, Stud. Surf. Sci. Catal. 75 (1993).
[38] M. Reit, R.G. Copperthwaite, G.J. Hutchings, J. Chem. Soc., Faraday Trans. 83 (9) (1987) 2963–2972.
[39] S.E. Colley, R.G. Copperthwaite, G.J. Hutchings, S.P. Terblanche, M.M. Thackeray, Nature 339 (1989) 129–130.
[40] R.B. Anderson, in: P.H. Emmett (Ed.), Catalysis IV, Reinhold, New York, 1956.
[41] E.L. Muetterties, Bull. Soc. Chim. Belg. 84 (1975) 959.
[42] M.G. Thomas, B.F. Beier, E.L. Muetterties, J. Am. Chem. Soc. 98 (5) (1976) 1296–1297.
[43] A. Brenner, D.A. Hucul, J. Am. Chem. Soc. 102 (7) (1980) 2484–2487.